

First Principles Model of a Tubular Photobioreactor for Microalgal Production

Ignacio Fernández,*[†] F. Gabriel Acién,*[‡] Manuel Berenguel,*[†] and José Luis Guzmán*[†]

*Department of Informatics, CIESOL, and [‡]Department of Chemical Engineering, University of Almería, International Excellence Campus ceiA3, E04120 Almería, Spain

ABSTRACT: This paper outlines and extends a dynamic model for microalgal production in outdoor tubular photobioreactors. A first principle based model, which takes into account both spatial and temporal gradients for the main culture variables, is presented. A previous model has been refined and extended in order to represent the main distributed phenomena, incorporating the dynamic effects related to culture temperature. Thereby, calibration and validation tests have been performed in an outdoor industrial tubular photobioreactor, showing successful results. The developed model considers both fluid dynamics and biological phenomena. This work summarizes the required steps to obtain a biological model from knowledge acquired in previous works. Finally, in view of the obtained results, conclusions about the limitations of the developed model are drawn, as well as its main uses and applications, describing a simulation example which proves how a simple control of culture conditions, such as temperature and pH, allows obtaining a higher biomass production rate.

INTRODUCTION

Microalgal production systems are receiving more attention year after year due to their potential in many industrial applications. Microalgal biomass is used to produce value-added bioproducts such as pharmaceuticals, animal feeds, or cosmetics, or even for human nutrition.^{1,2} On the other hand, other applications are focusing on the photosynthetic process performed by these microorganisms. In this way, the CO₂ from industrial plants can be fixed, mitigating the greenhouse gas emission as well as nitrogen or phosphorus in wastewater treatment processes obtaining environmental benefits.³ Finally, microalgal production is being used as a clean and renewable energy source (also called “third generation biofuels”), with a much higher yield than soybean crops and other biodiesel feedstocks, less spatial requirements, and a lack of competition for human consumption.^{4–6} For all these reasons, microalgae are considered as one of the main biodiesel feedstocks for the future by some authors.⁵ However, in order to be competitive in the bioenergy market, the cost and microalgal production capacity must be better than the rest of the biodiesel feedstocks.^{7,8}

Two widespread systems have been traditionally used to cultivate microalgae, from the simplest and less expensive ones, such as open ponds (well-known as “open raceways”) and lakes, where contamination-proof strains are cultivated with little control of its operating conditions, to highly controlled closed-culture systems called photobioreactors (PBRs), where high-value-added products are produced by strains more sensitive to contamination. Furthermore, PBRs allow a certain control level of operating conditions obtaining reproducible conditions for the culture.⁹ Nevertheless, the majority of these systems are built in a small scale medium obtaining a total worldwide biomass production around 9000 tonnes of dry matter per year, an insufficient quantity for the real worldwide demand for biodiesel fuel.^{10,11} Additionally, the production costs for these systems are nowadays too high to compete in bioenergy markets.

Currently, some studies from the biotechnology field have tried to reduce production costs by different ways, for instance by

means of the optimization of photobioreactor design and operation, by reducing the number of personnel to operate the plant, by using wastewater as a culture medium or carbon dioxide sources to incorporate it into the culture from industrial plants.^{7,8,12} However, all of them agree on the idea that an accurate optimization of the design, operation, control, and low-cost sources of nutrients are key to making this technology competitive with the rest of biodiesel feedstocks.

From a control point of view, some efforts have been devoted to controlling the pH, minimizing the control actions, and therefore reducing the CO₂ losses. When pure carbon is used, frequently demanded in PBRs, it can constitute up to 30% of the production cost,⁸ with losses up to 50% of gas injected, although it can be reduced by means of a proper design and operation of the photobioreactor below 30%.¹³ To further reduce the production cost of the system, it is necessary to employ advanced control strategies to ensure robustness, performance, and an optimization of the system.¹⁴ In addition, the mixing and mass transfer phenomena must be considered by this kind of strategy.¹⁵ Fernández et al.¹⁶ developed a simple approach by a classical proportional integral derivative (PID) plus feedforward strategy to control the pH of the culture, reducing significantly the cost and the CO₂ losses of the system against on-off controllers. On the other hand, Romero et al.¹⁷ used a filtered Smith predictor (FSP) for the same purpose, accounting for the time delay produced by the placement of a pH sensor. Moreover, techniques based on model predictive control (MPC) have obtained successful results in this target.^{18–21} An example can be found in Berenguel et al.,²² where a generalized predictive controller (GPC) was used to control the pH in a tubular photobioreactor. In that case, the performance of the controller was

Received: April 9, 2014

Revised: May 30, 2014

Accepted: June 2, 2014

Published: June 2, 2014

improved thanks to consideration of the on–off valve limitations. Also, other dynamics such as time delays or constraints can be taken into account, too. Nevertheless, the majority of these strategies are focused on only one control objective. To improve the system performance even further, it is necessary to take into account all system variables, and thus a cost reduction can be achieved by the proper utilization of resources. Ifrim et al.¹⁴ developed a nonlinear multivariable controller based on exact feedback linearization to control biomass concentration and the pH by means of controlling the dilution rate and the injected carbon dioxide gas flow rate. A mechanistic dynamical model was used for controller design purposes. In this line, some works have been addressed in other research fields, where the main control aim usually is related to productivity, economic issues, environmental, etc., with this problem being solved by a hierarchical control problem or optimal control strategies.^{23–28}

Depending on the control complexity, different types of system models are required. These models can range from the simplest ones, based on steady-state relationships or on linear low-order approaches, as shown by Fernández et al., Romero et al., and Berenguel et al.,^{16,17,22} to those based on nonlinear first principles.^{29–31} The last ones are addressed more to advanced control strategies, where an appropriate optimization of the whole system is performed in an upper layer. In addition, a dynamic nonlinear first principles based model of the system allows determination of experimental values for characteristic physicochemical parameters or even biological ones, being able to optimize the design and operation of photobioreactors. On the contrary, dynamic nonlinear first principles based models are very difficult to obtain due to the necessity of previous knowledge about the system, and above all, for biological systems, the large number of experimental tests needed to calibrate their parameters and their time-varying characteristic nature.

This work outlines and extends a dynamic model for microalgal culture based on physicochemical and biological principles, which predicts the three most important variables (temperature, pH, and dissolved oxygen) that influence the growth and performance of the culture in any microalgal production system. Furthermore, other system variables can be predicted, such as photosynthesis rate, biomass concentration, total inorganic carbon concentration, carbon dioxide concentration, oxygen and carbon dioxide molar fractions in the gas phase, and carbon dioxide losses. The model has been extended by improving the photosynthesis rate model and by taking into account the transport phenomena and the temperature of the culture. Several calibration and validation tests have been performed using an outdoor tubular photobioreactor. Since a large number of experimental test to calibrate biological models are necessary, this work presents some guidelines and recommendations. Moreover, comments about its main limitations are also included, determining its main fields of application.

The paper is organized as follows. In Materials and Methods a brief overview of the strain and photobioreactor used for the real experiments is presented. Then, the proposed model is explained, looking over balances reported previously by Fernández et al.³² and focusing on the distributed phenomena and the temperature balances added to represent its influence on the photosynthesis rate. Afterward, Results and Discussion presents the calibration and validation results of the proposed model. Discussions about the type of tests needed to obtain an accurate representation of the system and several applications of the model are provided, where a example of an application is proposed controlling the pH and temperature of the culture. Finally,

the paper ends with some conclusions, comments about the limitations, and main uses of the model and future works.

MATERIALS AND METHODS

Culture Conditions and Photobioreactor. The strain selected to be cultivated into the photobioreactor was *Scenedesmus almeriensis* (CCAP 276/24, Culture collection of Algae and Protozoa of the Center for Hydrology and Ecology, Ambleside, U.K.). This strain stands temperatures up to 45 °C and pH values up to 10, while its optimum conditions are 35 °C and pH 8.^{33,34} The experiments performed in this work took place in a tubular photobioreactor manipulated in continuous mode at a dilution rate of 0.34 L day⁻¹. The culture medium was Mann and Myers, prepared using agricultural fertilizers instead of pure chemicals. The microalgae were grown photoautotrophically with continuous aeration to avoid dissolved oxygen accumulation, under pH and temperature controlled conditions.

Experiments were performed on a tubular photobioreactor which belongs to a microalgal production facility, which is situated inside a greenhouse and located at the research center Estación Experimental Las Palmerillas, property of Cajamar Foundation (Almería, Spain). Ten tubular fence-type photobioreactors were built as described by Acién et al. and Molina et al.^{35,36} Figure 1 shows a view of this facility. The photobioreactor can be divided into two main parts (see Figure 2). On the one hand, the solar receiver is designed to maximize the interception of solar radiation, minimizing resistance to flow and occupying the minimum area as much as possible. On the other hand, a bubble column is used for mixing, degassing, and heat exchange culture. The total culture volume is 2600 L; the photobioreactor has 19.0 m length and 0.7 m width. The solar receiver is made of transparent tubes joined into a loop configuration to obtain a total horizontal length of 400 m and 0.09 m diameter. The microalgal culture is circulated at 1 m s⁻¹ using a centrifugal pump located between the bubble column and the solar receiver. The pH of the culture is controlled by on-demand injection of pure CO₂ at 5 L min⁻¹. The bubble column has 3.2 m height and 0.4 m inner diameter, and the dissolved oxygen is removed by a constant air flow rate of 140 L min⁻¹. Furthermore, the culture temperature is controlled through an internal heat exchanger located at the bubble column by passing cooling water at 1500 L h⁻¹. The culture is harvested at an overflow at the top of the column when fresh water is poured into the bubble column. Moreover, the pH, temperature, and dissolved oxygen are measured at several positions along the tube (three positions for dissolved oxygen, at the bottom, middle, and top of the photobioreactor; five positions for pH and temperature from the bottom to the top of the photobioreactor, being evenly distributed) using Crison probes (Crison Instruments, Spain), connected to a control-transmitter unit MM44 (Crison Instruments, Spain). Liquid and gas flow rates are measured using digital flow meters (PF2WS40 and PF2AS10 from SMC, Japan). Each measurement apparatus is in turn connected to a control computer through a data acquisition device, NI Compact FieldPoint (National Instruments, USA). The complete system was designed and built by the Department of Chemical Engineering at the University of Almería (Spain), and the control and data acquisition system was developed by the Department of Informatics at the University of Almería (Spain) using the development framework NI LabVIEW (LabVIEW 2011, National Instruments, USA).

First Principles Based Partial Differential Equation Model. Microalgal cultures are composed of liquids, gases, and



Figure 1. Real view of the tubular photobioreactor at the experimental station.

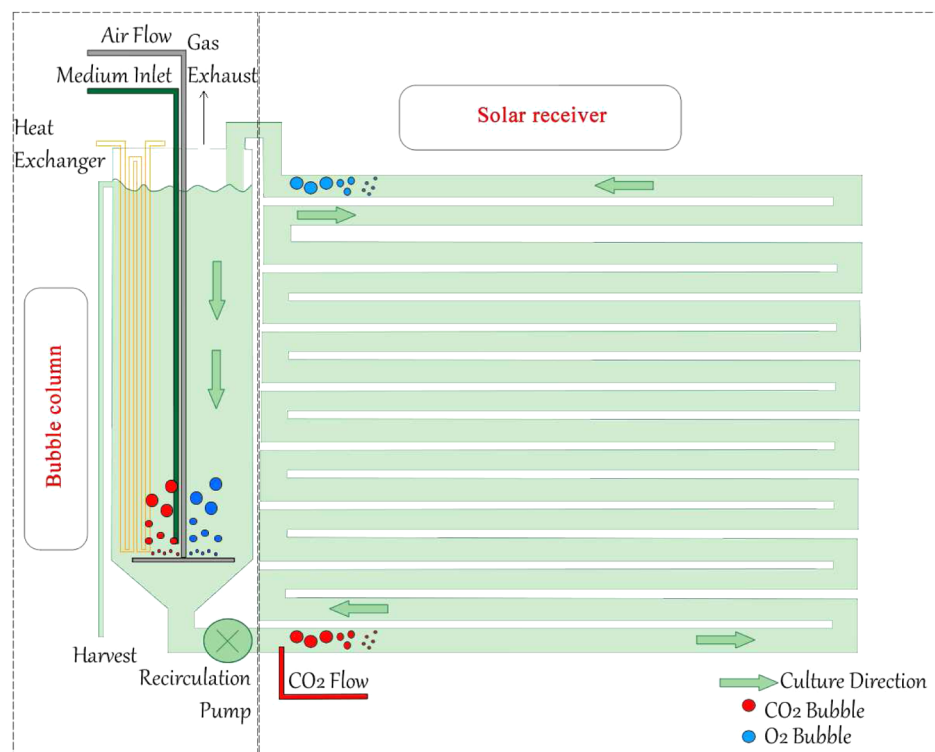


Figure 2. Tubular photobioreactor scheme.

single-cell phototrophic microorganisms (considered as part of the liquid fraction of the system), whose productivity depends on the culture conditions to which the cells are exposed. Therefore, a first principles based model must represent the physicochemical and biological phenomena that take place in the system, taking into account the relationships between light availability, culture conditions, and photosynthesis rate, besides the mixing and gas–liquid mass transfer inside the system. In outdoor cultures, the solar irradiance and temperature available depend on the location of the photobioreactor, while the rest of the nutrients needed for the cells depend on design and operating conditions of the photobioreactor. Thereby, a general growth model for the microalgal production system can be developed irrespective of the photobioreactor type. Growth can be modeled by a function of the photosynthesis rate. The main parameter that determines the photosynthesis rate is the available light, based on external irradiance, culture characteristics, and reactor geometry.^{13,37} The available light is calculated as a function of the total incident radiation on the photobioreactor surface, the light attenuation by biomass (Beer–Lambert law), and integrating local values over the total culture volume.³⁸ However, bearing in mind a specific geometry and photobioreactor, this function can be simplified by eq 1:^{38,39}

$$I_{av}(t, x) = \frac{I_0(t)\alpha}{K_a C_b(t, x)d_{t,p}}(1 - \exp(-K_a C_b(t, x)d_{t,p})) \quad (1)$$

where t is the time, x is the space, I_0 is the solar irradiance on an obstacle-free horizontal surface, K_a is the extinction coefficient, C_b is the biomass concentration, and $d_{t,p}$ is the tube diameter in the p part (where p can be substituted by “l” for the loop, solar receiver, and “c” for the bubble column). The solar irradiance has been modulated by a distribution factor α , which represents the solar irradiance fraction available in the particular area of the reactor.

The available average irradiance is correlated with the photosynthesis rate by a hyperbolic function as proposed by Molina et al. and Costache et al.^{38,40,41} This function is completed in this work by adding the rest of the factors that limit the microalgal growth (under sufficient conditions of nutrients). Therefore, the influence of the pH culture value, temperature, and dissolved oxygen of the culture have been modeled as described by Costache et al.⁴¹ Thus, a potential equation describes the influence of the dissolved oxygen concentration on the photosynthesis rate, whereas for the temperature and pH conditions two models based on the Arrhenius equation were selected. The complete version for the photosynthesis rate is described by eq 2:

$$P_{O_2}(t, x) = \frac{P_{O_{2,max}} I_{av}(t, x)^n}{K_i \exp(I_{av}(t, x)m) + I_{av}(t, x)^n} \left(1 - \left(\frac{[O_2](t, x)}{K_{O_2}} \right)^z \right) \left(B_1 \exp\left(\frac{-C_1}{pH(t, x)}\right) - B_2 \exp\left(\frac{-C_2}{pH(t, x)}\right) \right) \left(A_l \exp\left(\frac{-E_{a,1}}{RT(t, x)}\right) - A_2 \exp\left(\frac{-E_{a,2}}{RT(t, x)}\right) \right) - r P_{O_{2,max}} \quad (2)$$

where P_{O_2} is the photosynthesis rate (oxygen production rate per biomass mass unit), $P_{O_{2,max}}$ is the maximum photosynthesis rate

for microorganisms under the culture conditions, n is the form exponent, and the term in the denominator is the irradiance constant, which increases as an exponential function of average irradiance, and K_i and m are form parameters of this relationship. K_{O_2} is the oxygen inhibition constant and z is a form parameter. For the pH influence on the photosynthesis rate, B_1 and B_2 are the preexponential factors and C_1 and C_2 are the activation energies of the Arrhenius model, while A_l and A_2 and $E_{a,1s}$ and $E_{a,2}$ are the homologous variables for the temperature version. Furthermore, a factor r was included for the respiration phenomenon based on the maximum photosynthesis rate.

On the other hand, the carbon dioxide uptake, P_{CO_2} , can be expressed as a one-to-one molar ratio between oxygen and carbon dioxide as follows:

$$P_{CO_2}(t, x) = -P_{O_2}(t, x) \quad (3)$$

While the biological phenomena are represented by the equations described above, mixing, gas–liquid mass transfer, and heat transfer are explained in the next sections. The balances, for the solar receiver, are formulated by means of several partial differential equations (PDE) that lead to a distributed description of the process in the form of plug flow (approximation that allows finding a trade-off between model performance and computational cost). On the other hand, the bubble column is considered as stirred tank perfectly mixing, able to be modeled by ordinary differential equations (ODE), although a plug flow approach can be also used. The next subsections describe the mass balances reported by Fernández et al.,³² adding heat balances in order to consider the temperature of the system, and describing some improvements performed in the representation of the gas transport in the loop.

Mass Balances in the Liquid Phase. A mass balance for the biomass concentration can be defined as in eq 4, taking into account the photosynthesis process performed by the microalgal culture, and the transport phenomena due to the recirculation of the culture along the photobioreactor.

$$\begin{aligned} & A_{liq,l}(t, x) \frac{\partial C_b(t, x)}{\partial t} \\ &= -Q_{liq,l}(t, x) \frac{\partial C_b(t, x)}{\partial x} + A_{liq,l}(t, x) P_{O_2}(t, x) \\ & C_b(t, x) Y_{o/x} \end{aligned} \quad (4)$$

where the subscript “l” refers to the solar receiver. $A_{liq,l}$ is the cross-sectional liquid area in the solar receiver that can be calculated as $A_{t,l}(1 - \varepsilon_l(t,x))$, where $A_{t,l}$ is the total cross-sectional area of the loop and ε_l is the gas holdup. $Q_{liq,l}$ is the volumetric flow rate of liquid defined as $VA_{liq,l}$, where $V(t)$ is the velocity of the fluid established by the centrifugal pump of the photobioreactor, and $Y_{o/x}$ is the biomass yield coefficient produced by the oxygen unit mass.

In the bubble column, a similar balance can be considered by an ordinary differential equation where the spatial dimension is removed (although as has been pointed out before, plug flow could also be considered). Furthermore, since the dilution process is performed in this part of the photobioreactor, an output biomass concentration has been added driven by the volumetric flow rate of medium, eq 5.

$$\begin{aligned} V_{\text{liq},c}(t) \frac{dC_{\text{b,out}}(t)}{dt} \\ = -Q_{\text{liq},c}(t)(C_{\text{b,out}}(t) - C_{\text{b,in}}(t)) + V_{\text{liq},c}(t) P_{\text{O}_2}(t) \\ C_{\text{b,out}}(t) Y_{\text{o}/x} - Q_m(t) C_{\text{b,out}}(t) \end{aligned} \quad (5)$$

where the subscript "c" refers to the bubble column. $V_{\text{liq},c}$ is the liquid volume, which can be calculated as $V_{\text{t,c}}(1 - \epsilon_c)$, where $V_{\text{t,c}}$ is the total volume and ϵ_c is the gas holdup. $Q_{\text{liq},c}$ is the volumetric flow rate of liquid, $C_{\text{b,out}}$ is the outlet biomass concentration (solar receiver input), $C_{\text{b,in}}$ is the inlet biomass concentration (solar receiver output), and Q_m is the volumetric flow rate of culture medium.

Regarding dissolved oxygen concentration, it can be related to the gas–liquid mass transfer rate and the photosynthesis rate by the following mass balance:

$$\begin{aligned} A_{\text{liq,l}}(t, x) \frac{\partial [\text{O}_2](t, x)}{\partial t} \\ = -Q_{\text{liq,l}}(t, x) \frac{\partial [\text{O}_2](t, x)}{\partial x} \\ + A_{\text{liq,l}}(t, x) \frac{P_{\text{O}_2}(t, x) C_b(t, x)}{M_{\text{O}_2}} + A_{\text{liq,l}}(t, x) \\ K_l a_{l,\text{O}_2 l}(t, x) ([\text{O}_2^*](t, x) - [\text{O}_2](t, x)) \end{aligned} \quad (6)$$

where $[\text{O}_2]$ is the dissolved oxygen concentration in the liquid phase, M_{O_2} is the molecular weight of oxygen, $K_l a_{l,\text{O}_2 l}$ is the volumetric gas–liquid mass transfer coefficient for oxygen, and $([\text{O}_2^*] - [\text{O}_2])$ is the mean driving force. The equilibrium concentration in the gas phase $[\text{O}_2^*]$ is calculated as a function of the oxygen concentration in the gas phase based on Henry's law by eq 7:

$$[\text{O}_2^*](t) = H_{\text{O}_2} P_T y_{\text{O}_2}(t, x) \quad (7)$$

where H_{O_2} is Henry's constant for oxygen, P_T is the total pressure, and y_{O_2} is the oxygen molar fraction in the gas phase.

The homologous balance for the bubble column must consider the dissolved oxygen concentration in the input medium liquid. Thus, the next balance can be established:

$$\begin{aligned} V_{\text{liq},c}(t) \frac{d[\text{O}_2]_{\text{out}}(t)}{dt} \\ = -Q_{\text{liq},c}(t)([\text{O}_2]_{\text{out}}(t) - [\text{O}_2]_{\text{in}}(t)) \\ + V_{\text{liq},c}(t) \frac{P_{\text{O}_2}(t) C_{\text{b,out}}(t)}{M_{\text{O}_2}} + V_{\text{liq},c}(t) \\ K_l a_{l,\text{O}_2 c}(t) ([\text{O}_2^*](t) - [\text{O}_2](t))_{\text{lm}} \\ - Q_m(t)([\text{O}_2]_{\text{m}} - [\text{O}_2]_{\text{out}}(t)) \end{aligned} \quad (8)$$

where $[\text{O}_2]_{\text{in}}$ and $[\text{O}_2]_{\text{out}}$ are the oxygen concentrations in the liquid phase at the inlet and outlet of the bubble column, $K_l a_{l,\text{O}_2 c}$ is the volumetric gas–liquid mass transfer coefficient for oxygen in the bubble column, $([\text{O}_2^*] - [\text{O}_2])_{\text{lm}}$ is a logarithmic mean driving force, and $[\text{O}_2]_{\text{m}}$ is the dissolved oxygen in the culture medium.

Regarding inorganic total carbon concentration, it can be calculated by a mass balance to the liquid phase in a way similar to that for dissolved oxygen by eq 9.

$$\begin{aligned} A_{\text{liq,l}}(t, x) \frac{\partial [C_{\text{T}}](t, x)}{\partial t} \\ = -Q_{\text{liq,l}}(t, x) \frac{\partial [C_{\text{T}}](t, x)}{\partial x} \\ + A_{\text{liq,l}}(t, x) \frac{P_{\text{CO}_2}(t, x) C_b(t, x)}{M_{\text{CO}_2}} + A_{\text{liq,l}}(t, x) \\ K_l a_{l,\text{CO}_2 l}(t, x) ([\text{CO}_2^*](t, x) - [\text{CO}_2](t, x)) \end{aligned} \quad (9)$$

where $K_l a_{l,\text{CO}_2 l}$ is the mass transfer coefficient for CO_2 , and total inorganic carbon in the liquid phase is defined as $[C_{\text{T}}]$, which depends on the carbon dioxide concentration in the liquid phase $[\text{CO}_2]$ and the equilibrium concentration in the gas phase $[\text{O}_2^*]$. The equilibrium concentration can be calculated, according to Henry's law, as a function of Henry's constant, H_{CO_2} , the total pressure, P_T , and the molar fraction of CO_2 in the gas phase, y_{CO_2} .

For the bubble column, the inorganic carbon concentration from culture medium must be regarded in the balance as shown in eq 10.

$$\begin{aligned} V_{\text{liq},c}(t) \frac{d[C_{\text{T}}]_{\text{out}}(t)}{dt} \\ = -Q_{\text{liq},c}(t)([C_{\text{T}}]_{\text{out}}(t) - [C_{\text{T}}]_{\text{in}}(t)) \\ + V_{\text{liq},c}(t) \frac{P_{\text{CO}_2}(t) C_{\text{b,out}}(t)}{M_{\text{CO}_2}} + V_{\text{liq},c}(t) \\ K_l a_{l,\text{CO}_2 c}(t) ([\text{CO}_2^*](t) - [\text{CO}_2](t))_{\text{lm}} \\ - Q_m(t)([C_{\text{T}}]_{\text{m}} - [C_{\text{T}}]_{\text{out}}(t)) \end{aligned} \quad (10)$$

where $K_l a_{l,\text{CO}_2 c}$ is the mass transfer coefficient for CO_2 in the bubble column. The total inorganic carbon is defined at the inlet $[C_{\text{T}}]_{\text{in}}$ and outlet $[C_{\text{T}}]_{\text{out}}$ of the bubble column, and $[C_{\text{T}}]_{\text{m}}$ is the inorganic carbon concentration in the culture medium.

The pH value is defined as the decimal logarithm of the hydrogen concentration in the system, $-\log([\text{H}^+])$. Several equilibrium relations can be found between the hydrogen concentration and carbon species in the system (dissolved carbon dioxide, carbonate, $[\text{HCO}_3^-]$, and bicarbonate, $[\text{CO}_3^{2-}]$) as can be seen in Fernández et al.³²

Mass Balances in the Gas Phase. In addition to the liquid phase, CO_2 injections in gaseous form are incorporated in order to adjust the pH and neutralize the carbon lack in the system during the photosynthesis process. On the other hand, air injections are demanded in the bubble column to control high levels of dissolved oxygen accumulated in the loop. Therefore, mass balances on the gas phases are needed to include these phenomena. Since the nitrogen molar fraction can be considered constant because its solubility is approximately zero, the balances presented in this paper are formulated by relations from the rest of the gases to nitrogen molar ratio. Regarding the oxygen, the next balance, eq 11, can be established.

$$\begin{aligned} A_{\text{gas,l}}(t, x) \frac{\partial Y_{\text{O}_2}(t, x)}{\partial t} \\ = -\frac{F_{\text{N}_{2,l}}(t, x) V_{\text{mol}}}{Y_{\text{N}_{2,l}}} \frac{\partial Y_{\text{O}_2}(t, x)}{\partial x} - \frac{A_{\text{liq,l}}(t, x) V_{\text{mol}}}{Y_{\text{N}_{2,l}}} \\ \times K_l a_{l,\text{O}_2 l}(t, x) ([\text{O}_2^*](t, x) - [\text{O}_2](t, x)) \end{aligned} \quad (11)$$

where $A_{\text{gas},l}$ is the cross-sectional gas area, which can be calculated as $A_{t,c}\epsilon_l(t,x)$, V_{mol} is the molar volume under reactor conditions (pressure and temperature), Y_{O_2} is the oxygen to nitrogen molar ratio in the gas phase, $F_{\text{N}_{2,l}}$ is the molar flow rate of nitrogen in the gas phase, and $y_{\text{N}_{2,l}}$ is the nitrogen molar fraction used in the solar receiver. For the column, a similar mass balance can be considered taking into account the gas characteristics injected in this section. Thus, an ODE can be written as shown in eq 12.

$$\begin{aligned} V_{\text{gas},c}(t) \frac{dY_{\text{O}_2,\text{out}}(t)}{dt} \\ = -\frac{F_{\text{N}_{2,c}}(t)V_{\text{mol}}}{y_{\text{N}_{2,c}}}(Y_{\text{O}_2,\text{out}}(t) - Y_{\text{O}_2,\text{in}}(t)) \\ - \frac{V_{\text{liq},c}(t)V_{\text{mol}}}{y_{\text{N}_{2,c}}} K_l a_{l,\text{O}_2,c}(t)([\text{O}_2^*](t) - [\text{O}_2](t))_{\text{lm}} \end{aligned} \quad (12)$$

where the oxygen to nitrogen molar ratio in the gas phase is defined at the inlet $Y_{\text{O}_2,\text{in}}$ and outlet $Y_{\text{O}_2,\text{out}}$ of the bubble column, $V_{\text{gas},c}$ is the gas volume, which can be calculated as $V_{t,c}\epsilon_c(t)$, $F_{\text{N}_{2,c}}$ is the molar flow rate of nitrogen for the bubble column, and $y_{\text{N}_{2,c}}$ is the nitrogen molar fraction used in the bubble column. For the carbon dioxide, an analogous mass balance can be defined by eq 13.

$$\begin{aligned} A_{\text{gas},l}(t, x) \frac{\partial Y_{\text{CO}_2}(t, x)}{\partial t} \\ = -\frac{F_{\text{N}_{2,l}}(t, x)V_{\text{mol}}}{y_{\text{N}_{2,l}}} \frac{\partial Y_{\text{CO}_2}(t, x)}{\partial x} - \frac{A_{\text{liq},l}(t, x)V_{\text{mol}}}{y_{\text{N}_{2,l}}} \\ \times K_l a_{l,\text{CO}_2,l}(t, x)([\text{CO}_2^*](t, x) - [\text{CO}_2](t, x)) \end{aligned} \quad (13)$$

where Y_{CO_2} is the carbon dioxide to nitrogen molar ratio in the gas phase, $F_{\text{N}_{2,l}}$ is the molar flow rate of nitrogen in the gas phase, and $y_{\text{N}_{2,l}}$ is the nitrogen molar fraction used in the solar receiver. The perfectly mixing version for the bubble column is represented by eq 14.

$$\begin{aligned} V_{\text{gas},c}(t) \frac{dY_{\text{CO}_2,\text{out}}(t)}{dt} \\ = -\frac{F_{\text{N}_{2,c}}(t)V_{\text{mol}}}{y_{\text{N}_{2,c}}}(Y_{\text{CO}_2,\text{out}}(t) - Y_{\text{CO}_2,\text{in}}(t)) - \frac{V_{\text{liq},c}(t)V_{\text{mol}}}{y_{\text{N}_{2,c}}} \\ \times K_l a_{l,\text{CO}_2,c}(t)([\text{CO}_2^*](t) - [\text{CO}_2](t))_{\text{lm}} \end{aligned} \quad (14)$$

where the carbon dioxide to nitrogen molar ratio in the gas phase is defined at the inlet $Y_{\text{CO}_2,\text{in}}$ and outlet $Y_{\text{CO}_2,\text{out}}$ of bubble column.

In both mass balances, the molar ratio to nitrogen is used instead of the molar fraction. However, a relationship between these units is known by eq 15.

$$y = \frac{Y}{1 + Y} \quad (15)$$

An improvement has been developed taking into account the nitrogen gas transport because, although this element can be constant due to lack of mass transfer, a transport effect is produced when a gas bubble is injected in the loop up to when it finally leaves it. Assuming the same velocity for each component of the gas flow rate and no slip between the liquid phase and the gas phase, the gas transport can be modeled by changes in the

cross-sectional area of the nitrogen A_{N_2} along the tube, being able to describe these changes by the following balance:

$$A_{\text{gas},l}(t, x) \frac{\partial A_{\text{N}_2,l}(t, x)}{\partial t} = -\frac{F_{\text{N}_{2,l}}(t, x)V_{\text{mol}}}{y_{\text{N}_{2,l}}} \frac{\partial A_{\text{N}_2,l}(t, x)}{\partial x} \quad (16)$$

where $A_{\text{N}_2,l}$ is the cross-sectional area of the nitrogen in the solar receiver.

A relation can be found between the molar flow rate of nitrogen and the gas flow rate along the tube by eq 17.

$$F_{\text{N}_{2,l}}(t, x) = \frac{Q_{\text{gas},l}(t, x)y_{\text{N}_{2,l}}}{V_{\text{mol}}} \quad (17)$$

where the volumetric flow rate of gas $Q_{\text{gas},l}$ can be established as the sum of the three volumetric flow rates which take place in the loop (carbon dioxide, oxygen, and nitrogen). Therefore, a relationship between the volumetric flow rate of gas and the cross-sectional nitrogen area can be calculated using the molar ratio to nitrogen for the rest of components as

$$Q_{\text{gas}}(t, x) = VA_{\text{N}_2,l}(t, x)(1 + Y_{\text{O}_2}(t, x) + Y_{\text{CO}_2}(t, x)) \quad (18)$$

On the other hand, the gas holdup determines the mass transfer in both the bubble column and the solar receiver. Bearing in mind physical characteristics of each part of the system, different models of the gas holdup were modeled. For the solar receiver, assuming no slip between the liquid phase and the gas phase, the gas holdup expression can be approximated by eq 19.

$$\varepsilon_l(t, x) = \frac{Q_{\text{gas},l}(t, x)}{Q_{\text{gas},l}(t, x) + Q_{\text{liq},l}(t, x)} \quad (19)$$

In the bubble column, a slip velocity exists between the gas and liquid phases. Therefore, a drift flux model can be used to predict the gas holdup,⁴² which is given by eq 20.

$$\varepsilon_c(t) = \frac{U_{\text{gas},c}(t)}{(C_0 U_{\text{gas},c}(t) + U_{\text{liq},c}(t)) + U_\infty} \quad (20)$$

where $U_{\text{gas},c}$ and $U_{\text{liq},c}$ are the superficial velocity of the gas and liquid, respectively. C_0 is a drift flux model parameter, and U_∞ is the bubble accession rate.

Therefore, the mass transfer coefficient can be defined as a function of the gas holdup according to the part of the system that is modeled.⁴³ Even further, the mass transfer coefficient for the CO_2 is directly related to the mass transfer coefficient for the oxygen by the difference in aqueous diffusivity of the two gases (K_{CO_2}) as follows⁴⁴ in eqs 21 and 22.

$$\begin{aligned} K_l a_{l,\text{O}_2,l}(t, x) &= a_l \varepsilon_l(t, x)^{b_l} \\ K_l a_{l,\text{CO}_2,l}(t, x) &= K_{\text{CO}_2} K_l a_{l,\text{O}_2,l}(t, x) \\ K_l a_{l,\text{O}_2,c}(t) &= a_c \varepsilon_c(t)^{b_c} \quad K_l a_{l,\text{CO}_2,c}(t) = K_{\text{CO}_2} K_l a_{l,\text{O}_2,c}(t) \end{aligned} \quad (21) \quad (22)$$

$K_{\text{CO}_2,l}$ and $K_{\text{CO}_2,c}$ are the transfer coefficient constants for CO_2 at the solar receiver and at the bubble column, respectively; whereas a_l and b_l and a_c and b_c are form parameters adjusted to each part of the photobioreactor.

Another possible characterization of the mass transfer coefficients can be given by relating the volumetric interfacial area, eq 23, between the gas and the liquid phases.

$$K_l a_{l,O_2}(t, x) = K_l a_i(t, x) \quad (23)$$

where K_l is the liquid-side mass transfer coefficient; a_i is the interfacial area which can be calculated by the initial bubble diameter, d_b , and the gas holdup in each loop section as

$$a_i(t, x) = \frac{6\epsilon_l(t, x)}{d_b(1 - \epsilon_l(t, x))} \quad (24)$$

Temperature Balances. Temperature models are relevant for microalgal growth.^{45,46} In the case treated in this paper, as was mentioned in the section Culture Conditions and Photobioreactor, the culture temperature is controlled by a heat exchanger situated at the bubble column by passing cooling water. Heat balances have been developed in this section taking into account both fluid-dynamic and heat transfer phenomena, where the ambient temperature is considered uniform along the photobioreactor. The same methodology as for mass balances described above has been used; thus a temperature balance based on a plug flow model can be written as shown in eq 25.

$$\begin{aligned} C_p A_{liq,l}(t, x) \frac{\partial T(t, x)}{\partial t} \\ = -Q_{liq,l}(t, x) C_p \frac{\partial T(t, x)}{\partial x} + \alpha_l I_0(t) \pi d_l a \\ + h_l \pi d_{t,l} (T_{amb}(t) - T(t, x)) \end{aligned} \quad (25)$$

where C_p is the culture heat capacity, T is the temperature of the culture, I_0 is the solar irradiance modulated by a distribution factor α_l , $d_{t,l}$ is the loop diameter, a is a constant which represents the solar irradiance absorptivity, h_l is the coefficient of heat transmission between the ambient and the culture temperature, and T_{amb} is the ambient temperature which is considered homogeneous in the space.

Regarding the bubble column, the same balance is considered under the perfect mixing point of view, being established as follows in eq 26.

$$\begin{aligned} C_p V_{liq,c}(t) \frac{dT_{out}(t)}{dt} \\ = -Q_{liq,c}(t) C_p (T_{out}(t) - T_{in}(t)) + \alpha_c I_0(t) S_c a \\ + h_c S_c (T_{amb}(t) - T(t))_{lm} + h_{ext} S_{ext} (T_{ext}(t) - T(t))_{lm} \\ - Q_m(t) C_p (T_{out}(t) - T_m(t)) \end{aligned} \quad (26)$$

where T_{in} and T_{out} are the culture temperature at the inlet and outlet of the bubble column, α_c is the light distribution factor in the bubble column, h_c is the coefficient of heat transmission to the ambient in the bubble column, S_c is the column area available, h_{ext} is the coefficient of heat transmission between the heat exchanger situated in the bubble column and the culture temperature, S_{ext} is the heat exchanger area, T_{ext} is the temperature in the heat exchanger, and T_m is the temperature of culture medium.

On the other hand, a heat balance can be developed to obtain the output temperature expelled by the heat exchanger as follows:

$$C_p V_{ext} \frac{dT_{ext,out}(t)}{dt} = -Q_w(t) C_p (T_{ext,out}(t) - T_{ext,in}(t)) \\ - h_{ext} S_{ext} (T_{ext}(t) - T(t))_{lm} \quad (27)$$

where $T_{ext,in}$ and $T_{ext,out}$ are the culture temperature at the inlet and outlet of the heat exchanger, V_{ext} is the total volume of the heat exchanger, and Q_w is the volumetric flow rate of water that crosses through the heat exchanger.

RESULTS AND DISCUSSION

The calibration and validation of a biological system is a very complex task due to the large number of experimental tests that must be performed and the number of parameters that have to be calibrated, many of them depending on the culture conditions. For that reason, a suitable methodology is to divide these parameters into different groups depending on their characteristics; for example, biological and fluid-dynamic parameters can be separated in order to perform specific tests for each ones. Physical and chemical parameters, such as mass and heat transfer coefficients, can be determined by experimental data without culture or using known fluid-dynamic relationships.^{35,47} On the other hand, biological parameters can be calculated at the laboratory scale, where many conditions can be evaluated, although they must be readjusted in outdoor culture conditions and other scales.^{33,34,41} In addition, the whole system can be adjusted from experimental data of outdoor cultures, by fitting these data into the responses of the proposed model. Error metrics, such as integrated absolute error (IAE) or integrated squared error (ISE), can be used for this purpose, formulating an optimization problem for the calibration process. However, the use of experimental data of outdoor cultures must be treated carefully due to different reasons. First, noise and other disturbances must be filtered from the experimental data in order to remove possible uncertainties in the optimization problem. Second, the photosynthesis rate (eq 2), a biological part of the model, is an equation composed by different kinetic equations related to the culture conditions, and thus specific tests must be performed under controlled conditions for an appropriate calibration, such as was reported by Costache et al.⁴¹ However, this process is difficult to carry out in outdoor conditions, and therefore certain constraints and a suitable initial point, based on parameters obtained in laboratory scale, must be established in the calibration problem. Finally, possible disturbances must be considered, above all those affecting the pH variable. Since the pH value is very sensitive to changes in other variables such as total inorganic carbon, some disturbances can appear due to the inorganic carbon concentration added in the culture medium dilution during the operation in continuous mode, as well as small differences in the mass transfer coefficients because of biological reactions produced during the photosynthesis process.

From previous works presented in Costache et al. and Camacho et al.^{41,47} and significant knowledge of the system, experimental data from outdoor culture were only needed to fit the model response from biological parameters obtained in laboratory scale and fluid-dynamic parameters obtained from a similar photobioreactor structure (airlift-driven tubular photobioreactor). Thus, an optimization problem was solved using sequential quadratic programming (SQP) methods since a quadratic programming (QP) subproblem was formulated. A wide range of solar radiation conditions were covered (around 2 months of data with sunny and cloudy days), where the culture was operated in continuous mode at 0.34 L day⁻¹.

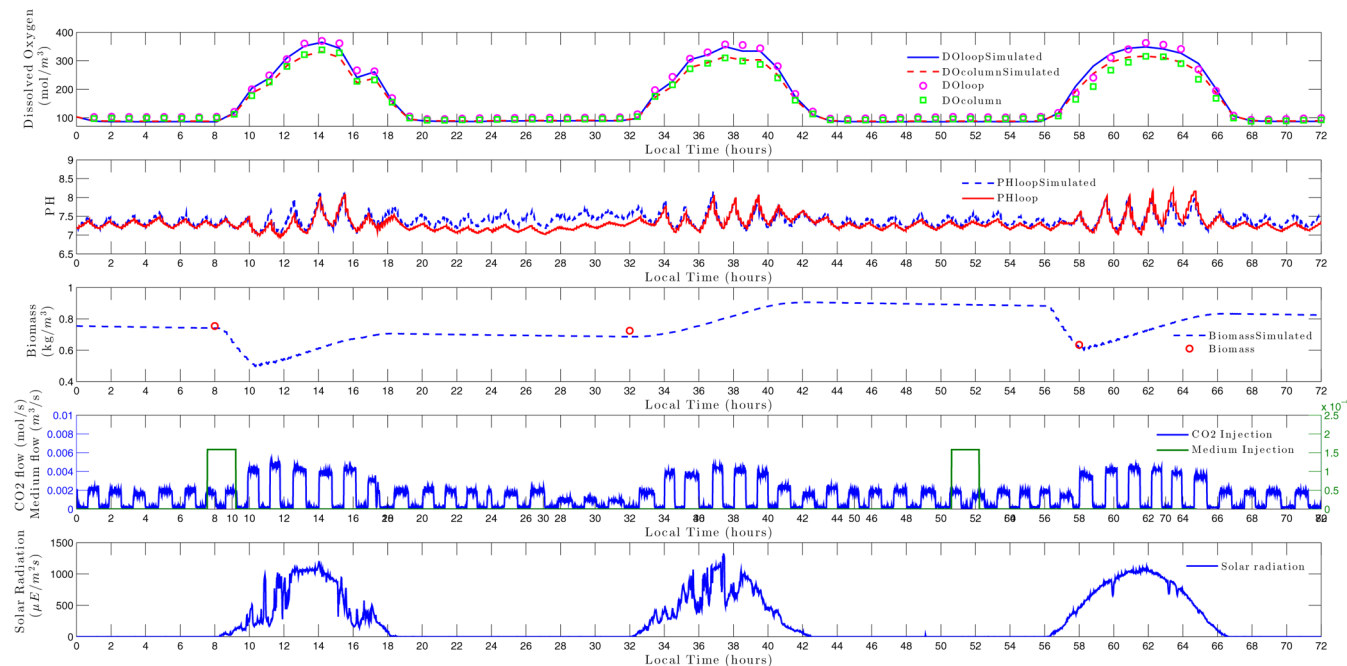


Figure 3. Calibration results: simulated and experimental data of dissolved oxygen concentration (DO), pH, and biomass concentration as a function of CO₂ injection and solar radiation (Feb 3–5, 2014).

The volumetric flow rate of air was constant at 140 L min⁻¹, allowing capture of the kinetic properties of the photosynthesis rate through the dissolved oxygen variable. The available data have been divided into two sets, one for calibration and another for validation purposes. Regarding CO₂ injections, an analysis on the pH was carried out in order to set up profiles of input signals that allow regulation of the pH, avoiding damages to the culture, and, at the same time, capturing dynamics related to CO₂ injection. Multilevel pseudorandom binary sequences (PRBS) were performed by a pulse-width modulation due to the discontinuous nature of the CO₂ valve; these signals were adapted according to the period of day to keep the pH value in an appropriate and secure range.^{33,34} The temperature of the culture was controlled by the volumetric flow rate of water and its temperature inside the heat exchanger. The volumetric flow rate is the actuator of the temperature controller, while the temperature of the water input depends on the temperature of water situated in a big reservoir for the whole plant. Several data were registered remaining the volumetric flow rate around 30 L min⁻¹. Finally, the velocity of the culture flow was fixed at 1 m s⁻¹ (notice that working with constant velocity is the typical way of operating these kinds of systems, although the developed model can cope with changing conditions on this variable).

The model was implemented in the Matlab environment. The PDE equations were solved by the method of lines using a backward finite difference approximation. The ODE equations for the bubble column were resolved by Runge–Kutta methods. It is important to take into account the relation between the time step, the space step, and the velocity of the system, $v(\Delta t/\Delta x)$, which is well-known as the Courant–Friedricks–Lowy or CFL number and must remain below or equal to unity. This condition must be satisfied to ensure stability and imposes limits in the computational cost.

Model Calibration and Validation. Regarding calibration and validation of the model, experimental data of solar radiation, biomass concentration, pH, dissolved oxygen, and temperature were required for calibration and validation steps. These problems

were divided into two periods: the night period when microalgae build up CO₂ due to respiration process, and the light period when the photosynthesis rate is produced and CO₂ is consumed. Mass transfer parameters for the loop section (a_l and b_l , eq 21) were calibrated with pH values (due to its higher influence on the CO₂ injections) during night periods, where the solar influence is neglected and therefore only mass transfer takes place. In the presence of radiation, parameters such as the light availability α (at both the loop α_l and bubble column α_c), the maximum photosynthesis rate $P_{O_2,max}$, form parameters K_i and m , and the exponent n were adjusted using the dissolved oxygen (eqs 1 and 2), whereas mass transfer parameters for the bubble column (a_c and b_c , eq 22) were calibrated by the difference between dissolved oxygen in the loop and in the bubble column, that is motivated by the influence of the air injection in the bubble column on the dissolved oxygen. On the other hand, the respiration rate (eq 2) was established from results to 1% of the maximum photosynthesis rate. Furthermore, several measurements of biomass concentration were used to adjust the biomass yield coefficient produced by the oxygen unit mass $Y_{O_2/x}$ (eqs 4 and 5). The rest of the parameters of eq 2 were maintained at values from the laboratory scale; it was necessary to perform an aggressive test that limits the growth rate of the culture (close to limit conditions) to fit these parameters appropriately. Regarding temperature (eqs 25 and 26), the solar irradiance absorptivity, a , and the heat transmission coefficients to the ambient, h_l and h_c , were fitted by means of temperature at the end of the loop and the bubble column, while the heat transmission coefficient to the heat exchanger (eq 27) was adjusted using the outlet temperature of the heat exchanger. The inputs used for this part of the model were the ambient temperature, medium temperature, water inlet temperature, volumetric flow rate of both water and medium inputs, and the solar irradiance. Other parameters, such as the tube diameter, culture heat capacity, and tube length, remained constants at values fixed by the design and previous knowledge of

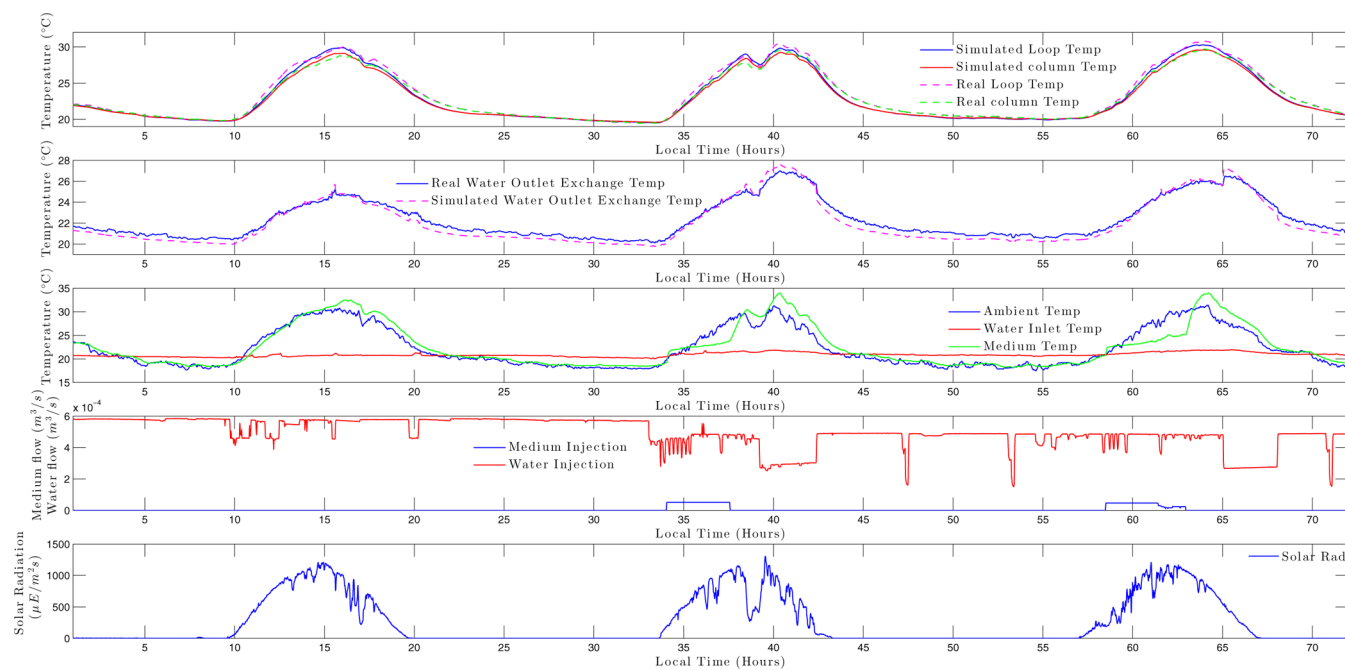


Figure 4. Calibration results: simulated and experimental data of temperature as a function of ambient temperature, medium temperature, water inlet temperature, volumetric flow rate of both water and medium inputs, and solar radiation (Oct 27–29, 2013).

the system; these parameters are shown in Table 2 in the Appendix.

Summarizing, the model is compound of two biological equations, eqs 1 and 2, where a total of 18 characteristic parameters must be calibrated in real conditions, although 10 of them ($z, K_{O_2}, B_1, C_1, B_2, C_2, A_1, A_2, E_{a,1}, E_{a,2}$), related to the factors of pH, dissolved oxygen, and temperature, have remained at values from the laboratory scale obtaining successful results. The rest of them ($a_b, a_o, K_o, P_{O_2,\max}, n, m, K_r, r$) have been calibrated by the procedure described in this work converging to an identifiable solution of these equations. Note that only the light availability parameter (a_l and a_c , eq 1) must be adjusted both for the solar receiver and for the bubble column due to the different solar exposition characteristics of each part. On the other hand, six mass balances (eqs 4, 6, 9, 11, 13, and 16) and one heat balance (eq 25) for the solar receiver, and five mass balances (eqs 5, 8, 10, 12, and 14) and two heat balances (eqs 26 and 27) for the bubble column represented the temporal and spacial physicochemical phenomena that take place in the photobioreactors, where four parameter (a_b, b_b, a, h_b) for the loop and four for the bubble column (a_o, b_o, h_o, h_{ext}) have been calibrated.

In Figures 3 and 4 some representative results of the calibration process are shown. Figure 3 shows both experimental and simulated concentrations of dissolved oxygen, pH, and biomass, while Figure 4 shows outlet temperature in the loop, bubble column, and heat exchange system. It can be seen how the model captures fast variations of the pH motivated by the CO_2 injections and the solar radiation, whereas smooth changes in dissolved oxygen and biomass concentration are also represented. As can be appreciated from Figure 5, the model reproduces clearly the closed loop nature of the system producing periodic oscillations related to the fluid velocity of the system, this being one of the improvements reached with the use of PDE equations to model the transport phenomena with respect to the model published in Fernández et al.³² The calibration results showed mean errors between simulated and experimental data of

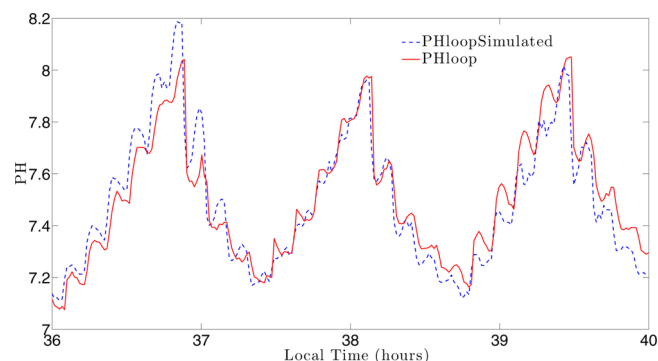


Figure 5. Enlarged view of calibration results.

6.92 and 4.99% for the dissolved oxygen (loop and bubble column, respectively), 1.65% for pH, and 3.44% for biomass concentration.

Regarding temperature, Figure 4 shows some calibration results for three consecutive days. In this case, the model represents slow changes regarding the culture temperature, mainly due to a higher time constant for this variable unlike the rest. The model suitably captures variations in the radiation profiles obtaining mean errors of 1.36% for the outlet culture temperature in the loop, 1.26% for the outlet culture temperature in the bubble column, and 1.42% in the outlet heat exchanger temperature.

Figure 6 and 8 show similar results for the validation process, where an average of the parametric values obtained in the calibration process were considered (these parameters are shown in Table 2 in the Appendix). The mean errors for this case were 3.43 and 10.81% for the dissolved oxygen, 1.56% for pH, and 2.81% for biomass concentration.

As for the rest of variables, an average of the parametric values was used for the culture temperature, obtaining the values described in Table 2. Figure 7 represents two representative days for the validation process. The solar irradiance absorptivity a was 0.54, while the heat coefficients of transmission to the

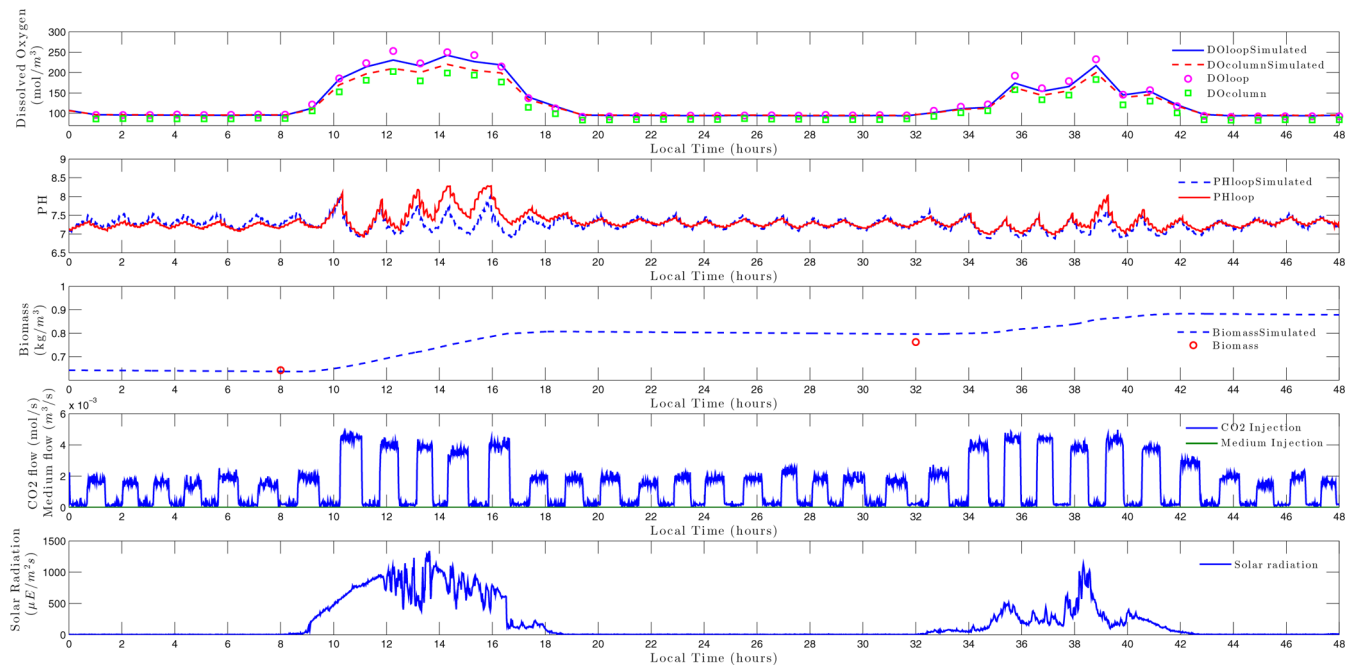


Figure 6. Validation results: simulated and experimental data of dissolved oxygen concentration (DO), pH, and biomass concentration as a function of CO_2 injection and solar radiation (Feb 25 and 26, 2014).

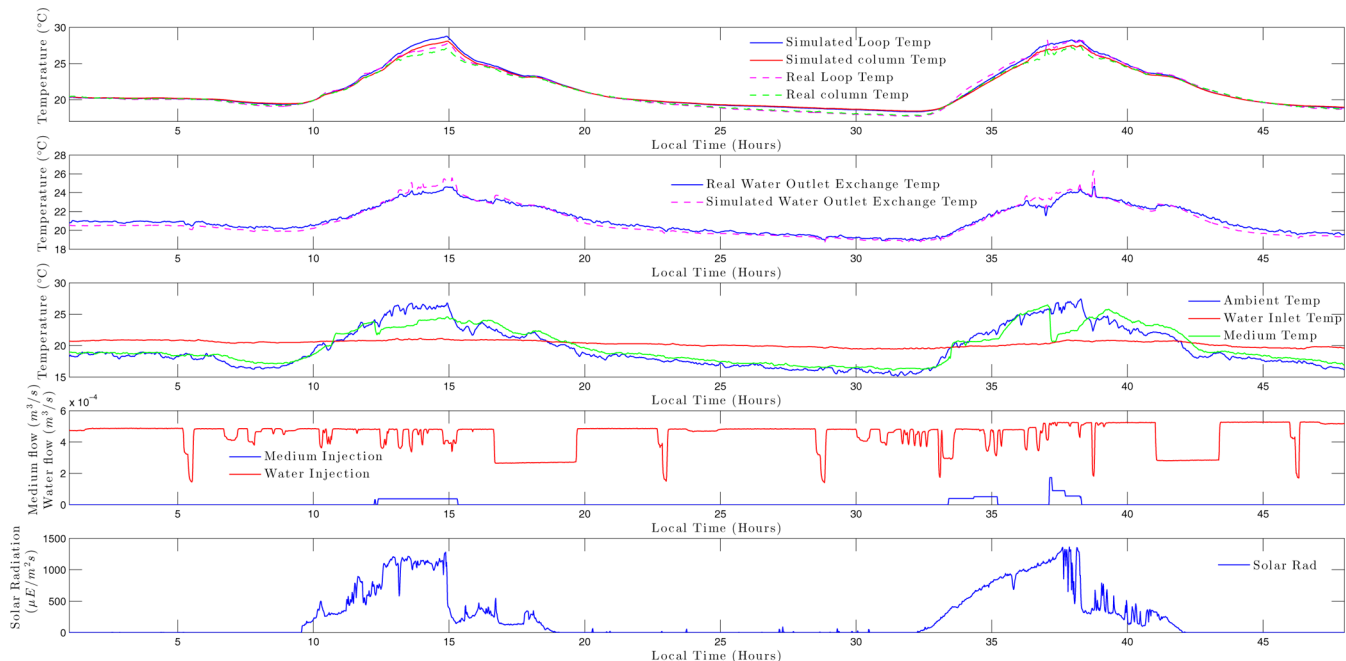


Figure 7. Validation results: simulated and experimental data of temperature as a function of ambient temperature, medium temperature, water inlet temperature, volumetric flow rate of both water and medium inputs, and solar radiation (Nov 19 and 20, 2013).

ambient in the bubble column h_c and in the loop h_l were 6.62 and $11.19 \text{ J s}^{-1} \text{ m}^{-2} \text{ }^\circ\text{C}^{-1}$, respectively. Finally, the heat coefficient of transmission to the heat exchanger h_{ext} was $450 \text{ J s}^{-1} \text{ m}^{-2} \text{ }^\circ\text{C}^{-1}$. The mean errors were 1.45% for the outlet culture temperature in the loop, 1.27% for the outlet culture temperature in the bubble column, and 1.84% for the outlet heat exchanger temperature.

The presented results can be considered a good approximation to the main system dynamics from the input–output point of view. Figure 9 shows a comparison between multiple measurement points located in different places of the loop. A CO_2 pulse was injected during the night (without solar irradiance), causing

periodic oscillations due to the closed loop nature of the system. It can be observed how the model reproduces this phenomenon, but the output of the model in the first cycle presents deviations from the real behavior mainly in the first sensors (those closer to the injection point). In view of these results, it can be concluded that in the first cycle, from the spatial point of view, the model should have to be improved by including molecular diffusion phenomena in the liquid phase to try to model this observed behavior.

The molecular diffusion can be modeled by Fick's second law, changing the structure of the liquid balances to consider both the

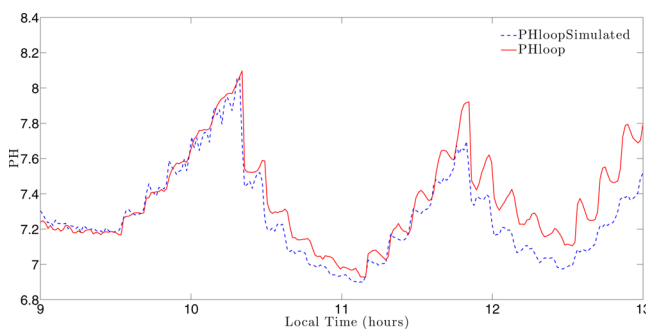


Figure 8. Enlarged view of validation results.

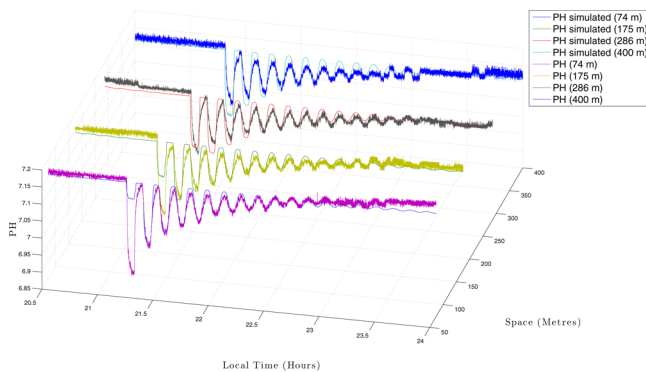


Figure 9. Effects of a CO_2 pulse on the pH spatial distribution.

convective flux and the molecular diffusion flux. This new structure is a complex mathematical equation that is well-known as the “diffusion–convection equation” (an example for the dissolved oxygen balance is shown by eq 28). An analytical solution taking into account initial and boundary conditions is given by Siemieniuch and Gladwell.⁴⁸ However, this does not satisfy the constructed boundary value problems for various boundary conditions. A numerical solution can be an alternative but with high computational cost.^{48,49} In this manner, an explicit finite difference solution can be achieved by the method of lines

using a second order central approximation (derived from the Taylor series) for the second derivative. In this case, a stable solution is found satisfying the constraints 29 and 30 (note that when $D_z \rightarrow 0$ the diffusion phenomenon is neglected obtaining the CFL constraint).

$$\begin{aligned} A_{\text{liq},l}(t, x) \frac{\partial [\text{O}_2](t, x)}{\partial t} \\ = -Q_{\text{liq},l}(t, x) \frac{\partial [\text{O}_2](t, x)}{\partial x} + D_z A_{\text{liq},l}(t, x) \times \frac{\partial^2 [\text{O}_2](t, x)}{\partial^2 x} A_{\text{liq},l}(t, x) \frac{P_{\text{O}_2}(t, x) C_b(t, x)}{M_{\text{O}_2}} \\ + A_{\text{liq},l}(t, x) K_l a_{\text{l},\text{O}_2}(t, x) ([\text{O}_2^*](t, x) - [\text{O}_2](t, x)) \end{aligned} \quad (28)$$

where D_z is the dispersion coefficient of the system and the stability constraints are given by

$$\frac{\Delta t}{\Delta x^2} \leq \frac{1}{2D_z} \quad (29)$$

$$\Delta t \leq \frac{2D_z}{V^2} \quad (30)$$

The problem is that, by including this phenomenon in the model, the computational cost strongly increases in such a way that it is impossible to perform a simulation in a reasonable time, much less calibration and validation procedures. Thus, it has been decided to reject the idea of including the diffusion phenomenon in the model in view of the desired application field discussed under Uses and Applications of the Model, leaving for future work the search of computationally affordable solutions to include the aforementioned phenomenon.

Uses and Applications of the Model. In this section, some uses and applications will be outlined. As can be seen above, the proposed model predicts the microalgal growth influenced by disturbances such as solar radiation and ambient temperature, which influence directly the culture conditions (pH, dissolved

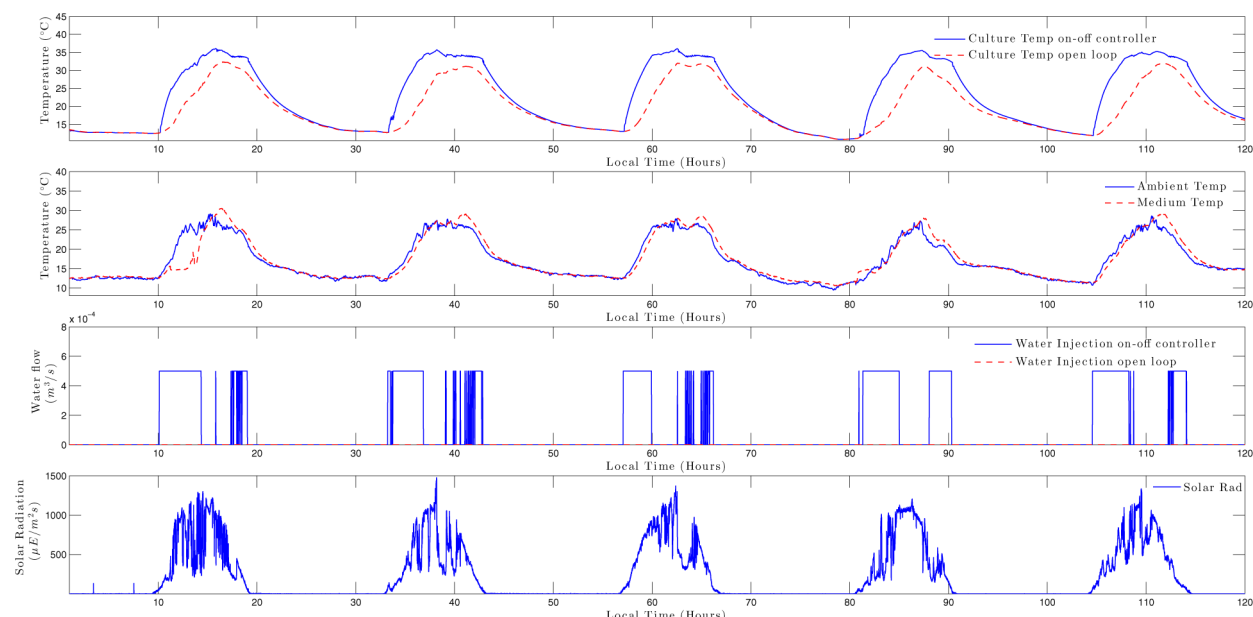


Figure 10. Scenario 1: temperature responses under winter conditions.

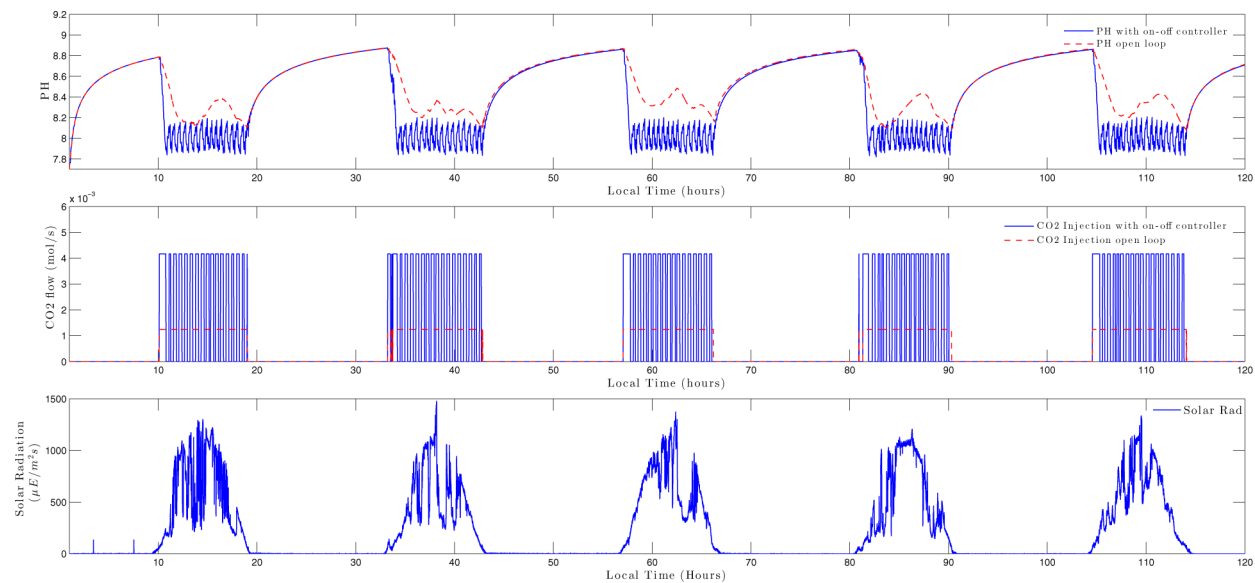


Figure 11. Scenario 1: pH responses under winter conditions.

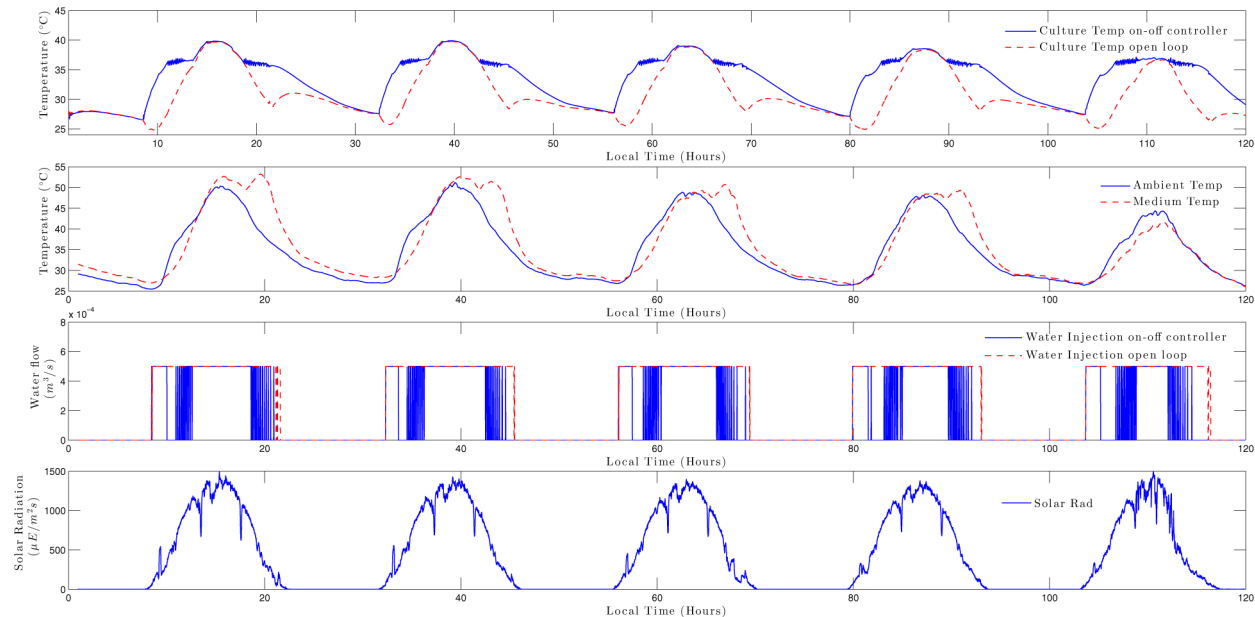


Figure 12. Scenario 2: temperature responses under summer conditions.

oxygen, and temperature). In addition to this, other system variables, which cannot be measured, are modeled such as carbon dioxide and total inorganic carbon concentrations, oxygen and carbon dioxide molar fractions in the gas phase, and even the carbon dioxide losses of the system. On the other hand, relations between the culture conditions and the inputs broadly used in any kind of microalgal system are taken into account. Below some examples of applications are described.

(a) The model can be considered as an useful tool in the optimization and design of photobioreactors, allowing performance of simulated studies for consecutive days in both discontinuous and continuous modes as can be seen in Figures 6 and 7.

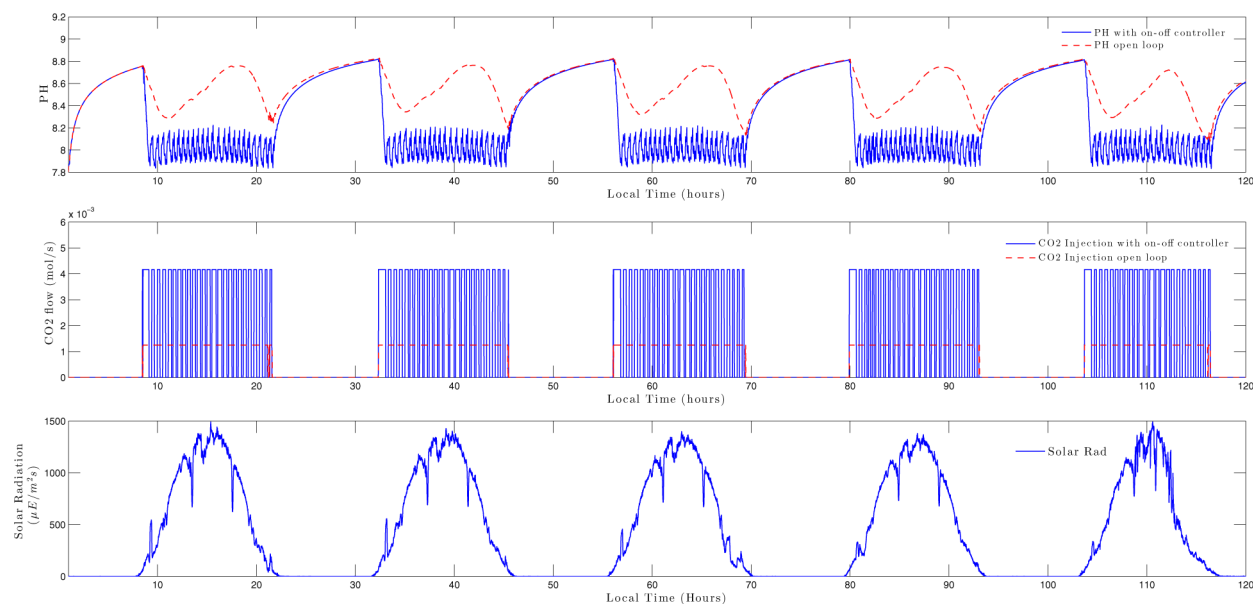
(b) The proposed model can be used as a virtual sensor, allowing prediction of unmeasured variables in a synchronous way to the real plant and obtaining real-time estimations.

(c) From a control point of view, a dynamic first principles based model provides a powerful tool to simulate any type of

control strategies. Although this paper is only focused on modeling aspects, a simple example is provided to show how this model can be used to evaluate control approaches. Therefore, the pH and temperature are controlled only by simple on–off controllers during five consecutive days (one scenario using winter conditions of radiation, Figures 10 and 11, and another one with summer conditions, Figures 12 and 13).

(d) Since the model is based on physical, chemical, and biological principles, it can be also used to elaborate optimal or hierarchical control strategies. In these kinds of strategies, the problem is divided into layers where the upper layer is focused on the resolution of an optimization problem, while the lower layer manages the information provided from the upper layer in order to manipulate local regulators.

Figures 10 and 11 show the control results for winter conditions. At the same time, these responses are compared with the open loop evolution of pH and temperature; a constant injection

**Figure 13.** Scenario 2: pH responses under summer conditions.**Table 1. Photosynthesis Rate and Biomass Production Rate Results for the Control Simulations of Figures 10–13**

day	Winter Results			
	oxygen generation mean rate, \overline{R}_{O_2} ($\text{kg m}^{-3} \text{ min}^{-1}$)		biomass production mean rate, \overline{P}_b ($\text{kg m}^{-3} \text{ min}^{-1}$)	
	without controller	on-off controller	without controller	on-off controller
1	1.2642×10^{-4}	1.5828×10^{-4}	1.2553×10^{-4}	1.5717×10^{-4}
2	1.2345×10^{-4}	1.5761×10^{-4}	1.2259×10^{-4}	1.5650×10^{-4}
3	1.2248×10^{-4}	1.8933×10^{-4}	1.5141×10^{-4}	1.8800×10^{-4}
4	1.2198×10^{-4}	1.6363×10^{-4}	1.2112×10^{-4}	1.6248×10^{-4}
5	1.3563×10^{-4}	1.7551×10^{-4}	1.3468×10^{-4}	1.7428×10^{-4}
total mean	1.3194×10^{-4}	1.6880×10^{-4}	1.3101×10^{-4}	1.6762×10^{-4}
Summer Results				
day	oxygen generation mean rate, \overline{R}_{O_2} ($\text{kg m}^{-3} \text{ min}^{-1}$)		biomass production mean rate, \overline{P}_b ($\text{kg m}^{-3} \text{ min}^{-1}$)	
	without controller	on-off controller	without controller	on-off controller
	3.4685×10^{-4}	3.6376×10^{-4}	3.4442×10^{-4}	3.6121×10^{-4}
1	3.4503×10^{-4}	3.6639×10^{-4}	3.4784×10^{-4}	3.6382×10^{-4}
2	3.4354×10^{-4}	3.6242×10^{-4}	3.4112×10^{-4}	3.5988×10^{-4}
3	3.3473×10^{-4}	3.5770×10^{-4}	3.3238×10^{-4}	3.5519×10^{-4}
4	2.8928×10^{-4}	3.1501×10^{-4}	2.8735×10^{-4}	3.1280×10^{-4}
5	3.3283×10^{-4}	3.5292×10^{-4}	3.3050×10^{-4}	3.5045×10^{-4}

of CO_2 to avoid the lack of carbon in the system is necessary. On the other hand, the mean value of the photosynthesis rate has been compared (see Table 1), showing clearly a higher photosynthesis rate, achieving a mean value for the five days of $1.6880 \times 10^{-4} \text{ kg m}^{-3} \text{ min}^{-1}$ when these conditions were controlled. This fact demonstrates the importance of an appropriate control of the culture conditions for an optimal system production and how the proposed model can be easily used to study and analyze these results.

Figures 12 and 13 show the same controllers during summer conditions. In this case, it has been necessary to inject a constant volumetric flow rate of water at 20°C to avoid extreme temperatures, for the open loop temperature evolution. From Table 1, the results related to the photosynthesis rate and the biomass production rate can be seen. As for winter conditions, on-off controllers reach higher values. However, the differences between the two proposed schemes are more noticeable during

winter conditions, proving the importance of heating the culture temperature in these periods.

CONCLUSIONS

A complete dynamic model for microalgal production is presented in this paper, which takes into account biological and fluid-dynamic phenomena that take place in any microalgal culture. The model is developed by first principles considering the distributed characteristics which are usual in microalgal production photobioreactors. Therefore, this model can be extended to other photobioreactor types. The uses and applications of the model are a design and operation tool for photobioreactors, virtual sensors for unmeasured variables, simulation framework, or a useful tool for analysis and design of advanced control strategies to an optimum plantwide control. Furthermore, in a simulation example, an increase of productivity has

Table 2. Parameters and Variables of the System

param/variable	description	value and units
a	solar irradiance x absorptivity	0.5411
a_i	interfacial area	m^{-1}
$A_{\text{gas},l}$	gas cross-sectional area of loop	m^2
$A_{\text{liq},l}$	liquid cross-sectional area of loop	m^2
$A_{t,c}$	total cross-sectional area of column	0.1257 m^2
$A_{t,l}$	total cross-sectional area of loop	0.0055 m^2
$A_{N_2,l}$	cross-sectional area of nitrogen gas in loop	m^2
a_c	form param in column	0.0806 s^{-1}
b_c	form param in column	0.7533
a_l	form param in loop	0.0012 s^{-1}
b_l	form param in loop	0.8450
A_1	preeponential factor	4.99×10^7
A_2	preeponential factor	1.66×10^{13}
B_1	preeponential factor	2.4098
B_2	preeponential factor	533.009
C_0	drift flux model param	0.996
C_1	activation energy	6.2684
C_2	activation energy	68.8062
C_b	biomass concn	kg m^{-3}
$[\text{CO}_{2,p}]$	carbon dioxide concn in liquid phase in solar receiver	mol m^{-3}
$[\text{CO}_2^*]$	equilib concn with gas phase for dioxide carbon	mol m^{-3}
$[\text{CO}_3^{2-}]$	bicarbonate species	mol m^{-3}
$[\text{C}_T]$	total inorganic carbon concn	mol m^{-3}
$[\text{C}_T]_m$	total inorganic carbon in medium	8 mol m^{-3}
C_p	volumetric heat capacity	$1 \text{ kcal m}^{-3} \text{ }^\circ\text{C}^{-1}$
d_b	bubble diameter	m
$d_{t,c}$	total column diameter	0.4 m
$d_{t,l}$	total loop diameter	0.084 m
D_z	dispersion coeff	$\text{m}^2 \text{ s}^{-1}$
$E_{a,1}$	activation energy	$4.27 \times 10^4 \text{ mol J}^{-1}$
$E_{a,2}$	activation energy	$7.71 \times 10^4 \text{ mol J}^{-1}$
$F_{N_2,l}$	molar flow of nitrogen for gas phase in loop	mol s^{-1}
$[\text{H}^+]$	hydrogen species	mol m^{-3}
H_{CO_2}	Henry's const for carbon dioxide	$38.36 \text{ mol atm}^{-1} \text{ m}^{-3}$
H_{O_2}	Henry's const for oxygen	$1.07 \text{ mol atm}^{-1} \text{ m}^{-3}$
$[\text{HCO}_3^-]$	carbonate species	mol m^{-3}
h_c	transmission coeff to ambient in bubble column	$11.1886 \text{ J s}^{-1} \text{ m}^{-2} \text{ }^\circ\text{C}^{-1}$
h_l	transmission coeff to ambient in loop	$6.6189 \text{ J s}^{-1} \text{ m}^{-2} \text{ }^\circ\text{C}^{-1}$
h_{ext}	transmission coeff to heat exchanger	$449.9170 \text{ J s}^{-1} \text{ m}^{-2} \text{ }^\circ\text{C}^{-1}$
I_{av}	average solar irradiance	$\mu\text{E m}^{-2} \text{ s}^{-1}$
I_0	solar irradiance on an horizontal surface	$\mu\text{E m}^{-2} \text{ s}^{-1}$
K_a	extinction coeff	$133.0324 \text{ m}^2 \text{ kg}^{-1}$
$K_{\text{CO}_{2,c}}$	transfer coeff const for CO_2 in column	0.91
$K_{\text{CO}_{2,l}}$	transfer coeff const for CO_2 in loop	0.91
K_i	form param	$173.9504 \mu\text{E m}^{-2} \text{ s}^{-1}$
K_l	liquid-side mass transfer coeff	m s^{-1}
$K_{\text{la}_{\text{CO}_2,c}}$	volumetric gas–liquid mass transfer coeff for CO_2 in column	s^{-1}
$K_{\text{la}_{\text{CO}_2,l}}$	volumetric gas–liquid mass transfer coeff for CO_2 in solar receiver	s^{-1}
$K_{\text{la}_{\text{O}_2,c}}$	volumetric gas–liquid mass transfer coeff for O_2 in column	s^{-1}

Table 2. continued

param/variable	description	value and units
$K_{\text{la}_{\text{O}_2,l}}$	volumetric gas–liquid mass transfer coeff for O_2 in solar receiver	s^{-1}
K_{O_2}	oxygen inhibition const	$0.7202 \text{ mol m}^{-3}$
L_c	length of column	3.2 m
L_l	length of loop	400 m
m	form param	0.0015
M_{CO_2}	molecular weight of carbon dioxide	32 g mol^{-1}
M_{O_2}	molecular weight of oxygen	44 g mol^{-1}
n	form exponent	0.9779
$[\text{O}_2]$	dissolved oxygen concn	mol m^{-3}
$[\text{O}_2^*]$	equilb concn with gas phase for oxygen	mol m^{-3}
$[\text{O}_2]_m$	dissolved oxygen in medium	$0.2812 \text{ mol m}^{-3}$
P_{CO_2}	carbon dioxide consumption rate	$\text{kg of CO}_2 \text{ kg}^{-1} \text{ s}^{-1}$
P_{O_2}	photosynthesis rate	$\text{kg of O}_2 \text{ kg}^{-1} \text{ s}^{-1}$
$P_{\text{O}_2,\text{max}}$	maximum photosynthesis rate	$4.37 \times 10^{-5} \text{ kg of O}_2 \text{ kg}^{-1} \text{ s}^{-1}$
P_T	total pressure	1 atm
$Q_{\text{gas},l}$	volumetric flow rate of gas in loop	$\text{m}^3 \text{ s}^{-1}$
$Q_{\text{liq},l}$	volumetric flow rate of liquid in loop	$\text{m}^3 \text{ s}^{-1}$
Q_m	volumetric flow rate of culture medium	$\text{m}^3 \text{ s}^{-1}$
Q_w	volumetric flow rate of water crossing in heat exchanger	$\text{m}^3 \text{ s}^{-1}$
r	respiration factor	0.01
R	gas constant	$\text{J mol}^{-1} \text{ K}^{-1}$
S_c	column area	4.0212 m^2
S_{ext}	heat exchanger area	3.1919 m^2
t	time	s
T	culture temp	$^\circ\text{C}$
T_{amb}	ambient temp	$^\circ\text{C}$
T_{ext}	heat exchanger temp	$^\circ\text{C}$
T_m	medium temp	$^\circ\text{C}$
U_∞	bubble accession rate	0.651 m s^{-1}
U_{gas}	superficial velocity of gas	0.0186 m s^{-1}
U_{liq}	superficial velocity of liquid	0.0441 m s^{-1}
V	velocity of fluid	1 m s^{-1}
$V_{\text{liq},c}$	liquid bubble column vol	m^3
$V_{\text{gas},c}$	gas bubble column vol	m^3
$V_{t,c}$	total bubble column vol	0.4021 m^3
$V_{t,l}$	total loop vol	2.2167 m^3
V_{mol}	molar vol	20 L mol^{-1}
V_{ext}	heat exchanger vol	20.3 L
x	longitudinal space along loop	m
y_{CO_2}	carbon dioxide molar fraction	
Y_{CO_2}	CO_2 to N_2 molar ratio in gas phase	$\text{mol of CO}_2 / (\text{mol of N}_2)$
y_{N_2}	nitrogen molar fraction	
y_{O_2}	oxygen molar fraction	
Y_{O_2}	O_2 to N_2 molar ratio in gas phase	$\text{mol of O}_2 / (\text{mol of N}_2)$
$Y_{\text{o/x}}$	biomass yield coeff	$0.9713 \text{ kg kg}^{-1} \text{ of O}_2$
z	form param	5.4333
α	distribution solar factor	
α_c	distribution solar factor for bubble column	0.1052
α_l	distribution solar factor for solar receiver	0.9725
ε_l	gas holdup loop in solar receiver	
ε_c	gas holdup in the bubble column	

been demonstrated by a simple control of the pH and temperature conditions.

Future efforts will concentrate on finding numerical solutions to the diffusion equations with acceptable computational costs to fully include this effect in the model and also to determine optimal placement of sensors in the installation. The biological part of the model will also be extended to try to represent the "aging" state of the culture.

APPENDIX

Table 2 includes fixed values of parameters and variables for the system in this work.

AUTHOR INFORMATION

Corresponding Authors

*E-mail: ifernandez@ual.es.

*E-mail: facien@ual.es.

*E-mail: beren@ual.es.

*E-mail: joseluis.guzman@ual.es.

Notes

The authors declare no competing financial interest.

ACKNOWLEDGMENTS

This work has been partially funded by the projects DPI2011-27818-C02-01 (financed by the Spanish Ministry of Science and Innovation and EU-ERDF funds), Controlcrop PIO-TEP-6174 (financed by the Consejería de Economía, Innovación y Ciencia de la Junta de Andalucía), and CENIT VIDA (financed by the Spanish Ministry of Economy and Competitiveness and CDTI funds), and supported by Cajamar Foundation.

REFERENCES

- Pulz, O.; Gross, W. Valuable products from biotechnology of microalgae. *Appl. Microbiol. Biotechnol.* **2004**, *65*, 635–648.
- Spolaore, P.; Joannis-Cassan, C.; Duran, E.; Isambert, A. Commercial applications of microalgae. *J. Biosci. Bioeng.* **2006**, *101*, 87–96.
- Wang, B.; Li, Y.; Wu, N.; Lan, C. Q. CO₂ bio-mitigation using microalgae. *Appl. Microbiol. Biotechnol.* **2008**, *79*, 707–718.
- Chisti, Y. Biodiesel from microalgae. *Biotechnol. Adv.* **2007**, *25*, 294–306.
- Bernard, O. Hurdles and challenges for modelling and control of microalgae for CO₂ mitigation and biofuel production. *J. Process Control* **2011**, *21*, 1378–1389.
- Mata, T. M.; Martins, A. A.; Caetano, N. S. Microalgae for biodiesel production and other applications: a review. *Renewable Sustainable Energy Rev.* **2010**, *14*, 217–232.
- Acién, F. G.; González, C. V.; Fernández, J. M.; Molina, E. Conversion of CO₂ into biomass by microalgae: how realistic a contribution may it be to significant CO₂ removal? *Appl. Microbiol. Biotechnol.* **2012**, *96*, 577–586.
- Acién, F. G.; Fernández, J. M.; Magán, J. J.; Molina, E. Production cost of a real microalgae production plant and strategies to reduce it. *Biotechnol. Adv.* **2012**, *30*, 1344–1353.
- Wang, B.; Lan, C. Q.; Horsman, E. Closed photobioreactors for production of microalgal biomasses. *Biotechnol. Adv.* **2012**, *30*, 904–912.
- Brennan, L.; Owende, P. Biofuels from microalgae: a review of technologies for production, processing, and extractions of biofuels and co-products. *Renewable Sustainable Energy Rev.* **2010**, *14*, 557–577.
- Taras, S.; Woinaroschy, A. An interactive multi-objective optimization framework for sustainable design of bioprocesses. *Comput. Chem. Eng.* **2012**, *43*, 10–22.
- Norsker, N. H.; Barbosa, M. J.; Vermüë, M. H.; Wijffels, R. H. Microalgal production: a close look at the economics. *Biotechnol. Adv.* **2011**, *29*, 24–27.
- Acién, F. G.; García, F.; Chisti, Y. Photobioreactors: light regime, mass transfer, and scaleup. *Prog. Ind. Microbiol.* **1999**, *35*, 231–247.
- Ifrim, G. A.; Titica, M.; Barbu, M.; Boillereaux, L.; Cogne, G.; Caraman, S.; Legrand, J. Multivariable feedback linearizing control of *Chlamydomonas reinhardtii* photoautotrophic growth process in a torus photobioreactor. *Chem. Eng. J.* **2013**, *218*, 191–203.
- García, J. L.; Berenguel, M.; Rodríguez, F.; Fernández, J. M.; Brindley, C.; Acién, F. G. Minimization of carbon losses in pilot-scale outdoor photobioreactors by model-based predictive control. *Bio-technol. Bioeng.* **2003**, *84*, 533–543.
- Fernández, I.; Peña, J.; Guzmán, J. L.; Berenguel, M.; Acién, F. G. Modelling and control issues of pH in tubular photobioreactors. *Proceedings of the 11th IFAC Symposium on Computer Applications in Biotechnology, CAB 2010, Leuven, Belgium*; International Federation of Automatic Control: Laxenburg, Austria, 2010.
- Romero-García, J. M.; Guzmán, J. L.; Moreno, J. C.; Acién, F. G.; Fernández, J. M. Filtered Smith Predictor to control pH during enzymatic hydrolysis of microalgae to produce L-aminoacids concentrates. *Chem. Eng. Sci.* **2012**, *82*, 121–131.
- Kumar, A. S.; Ahmad, Z. Model predictive control (MPC) and its current issues in chemical engineering. *Chem. Eng. Commun.* **2012**, *199*, 472–511.
- Oblak, S.; Škrjanc, I. Continuous-time Wiener-model predictive control of a pH process based on a PWL approximation. *Chem. Eng. Sci.* **2010**, *65*, 1720–1728.
- Lazar, C.; Pintea, R.; Keyser, R. D. Nonlinear predictive control of a pH process. *17th European Symposium on Computer Aided Process Engineering, ESCAPE17, Bucharest, Romania*; Plesu, V., Agachi, P. S., Eds.; Elsevier: Amsterdam, The Netherlands, 2007; pp 829–834.
- Christofides, P. D.; Scattolini, R.; de la Peña, D. M.; Liu, J. Distributed model predictive control: A tutorial review and future research directions. *Comput. Chem. Eng.* **2013**, *51*, 21–41.
- Berenguel, M.; Rodríguez, F.; Acién, F. G.; García, J. L. Model predictive control of pH in tubular photobioreactors. *J. Process Control* **2004**, *14*, 377–387.
- Scattolini, R. Architectures for distributed and hierarchical Model Predictive Control—A review. *J. Process Control* **2009**, *19*, 723–731.
- Ramírez, A.; Rodríguez, F.; Guzmán, J. L.; Berenguel, M. Multiobjective hierarchical control architecture for greenhouse crop growth. *Automatica* **2012**, *48*, 490–498.
- Camacho, E.; Rubio, F.; Berenguel, M.; Valenzuela, L. A survey on control schemes for distributed solar collector fields. Part I: Modeling and basic control approaches. *Sol. Energy* **2007**, *81*, 1240–1251.
- Camacho, E.; Rubio, F.; Berenguel, M.; Valenzuela, L. A survey on control schemes for distributed solar collector fields. Part II: Advanced control approaches. *Sol. Energy* **2007**, *81*, 1252–1272.
- Grognard, F.; Akhmetzhanov, A. R.; Bernard, O. Optimal strategies for biomass productivity maximization in a photobioreactor using natural light. *Automatica* **2014**, *50*, 359–368.
- Gong, J.; You, F. Optimal design and synthesis of algal biorefinery processes for biological carbon sequestration and utilization with zero direct greenhouse gas emissions: MINLP model and global optimization algorithm. *Ind. Eng. Chem. Res.* **2014**, *53*, 1563–1579.
- Nauha, E. K.; Alopaeus, V. Modeling method for combining fluid dynamics and algal growth in a bubble column photobioreactor. *Chem. Eng. J.* **2013**, *229*, 559–568.
- Yang, A. Modeling and evaluation of CO₂ supply and utilization in algal ponds. *Ind. Eng. Chem. Res.* **2011**, *50*, 11181–11192.
- Vunjak-Novakovic, G.; Kim, Y.; Wu, X.; Berzin, I.; Merchuk, J. C. Air-Lift bioreactors for algal growth on flue gas: Mathematical modeling and pilot-plant studies. *Ind. Eng. Chem. Res.* **2005**, *44*, 6154–6163.
- Fernández, I.; Acién, F. G.; Fernández, J. M.; Guzmán, J. L.; Magán, J. J.; Berenguel, M. Dynamical model of microalgal production in tubular photobioreactors. *Bioresour. Technol.* **2012**, *126*, 172–281.
- Sánchez, J. F.; Fernández, J. M.; Acién, F. G.; Rueda, A.; Pérez, J.; Molina, E. Influence of culture conditions on the productivity and lutein content of the new strain *Scenedesmus almeriensis*. *Process Biochem.* **2008**, *43*, 398–405.

- (34) Sánchez, J. F.; Fernández, J. M.; Acién, F. G.; Cerón, M. C.; Pérez, J.; Molina, E. Biomass and lutein productivity of *Scenedesmus almeriensis*: influence of irradiance, dilution rate and temperature. *Appl. Microbiol. Biotechnol.* **2008**, *79*, 719–729.
- (35) Acién, F. G.; Fernández, J. M.; Sánchez, J. A.; Molina, E.; Chisti, Y. Airlift-driven external-loop tubular photobioreactors for outdoor production of microalgae: assessment of design and performance. *Chem. Eng. Sci.* **2001**, *S6*, 2721–2732.
- (36) Molina, E.; Fernández, J.; Acién, F. G.; Chisti, Y. Tubular photobioreactor design for algal cultures. *J. Biotechnol.* **2001**, *92*, 113–131.
- (37) Acién, F. G.; Fernández, J. M.; Molina, E. Photobioreactors for the production of microalgae. *Rev. Environ. Sci. Bio/Technol.* **2013**, *12*, 131–151.
- (38) Molina, E.; Sevilla, J. M.; Pérez, J. A.; Camacho, F. G. A study on simultaneous photolimitation and photoinhibition in dense microalgal cultures taking into account incident and averaged irradiances. *J. Biotechnol.* **1996**, *45*, 59–69.
- (39) Acién, F. G.; García, F.; Sánchez, J. A.; Fernández, J. M.; Molina, E. A model for light distribution and average solar irradiance inside outdoor tubular photobioreactors for the microalgal mass culture. *Biotechnol. Bioeng.* **1997**, *55*, 701–714.
- (40) Molina, E.; García, F.; Sánchez, J. A.; Acién, F. G.; Fernández, J. M. Growth yield determination in a chemostat culture of the marine microalga *ochrysis galbana*. *J. Appl. Phycol.* **1996**, *8*, 529–534.
- (41) Costache, T. A.; Acién, F. G.; Morales, M. M.; Fernández, J. M.; Stamatin, I.; Molina, E. Comprehensive model of microalgae photosynthesis rate as a function of culture conditions in photobioreactors. *Appl. Microbiol. Biotechnol.* **2013**, *1*–11.
- (42) Zuber, N.; Findlay, J. A. Average Volumetric Concentration in Two-Phase Flow Systems. *J. Heat Transfer* **1965**, *87*, 453–468.
- (43) Chisti, M. Y.; Moo-Young, M. Airlift reactors: characteristics, applications and design considerations. *Chem. Eng. Commun.* **1987**, *60*, 195–242.
- (44) Molina, E.; Sánchez, J. A.; García, F.; Robles, A. Gas–liquid transfer of atmospheric CO₂ in microalgal cultures. *J. Chem. Technol. Biotechnol.* **1993**, *S6*, 329–337.
- (45) Goetz, V.; Borgne, F. L.; Pruvost, J.; Plantard, G.; Legrand, J. A generic temperature model for solar photobioreactors. *Chem. Eng. J.* **2011**, *175*, 443–449.
- (46) Ras, M.; Steyer, J. P.; Bernard, O. Temperature effect on microalgae: a crucial factor for outdoor production. *Rev. Environ. Sci. Bio/Technol.* **2013**, *12*, 153–164.
- (47) Camacho, F.; Acién, F. G.; Sánchez, J. A.; García, F.; Molina, E. Prediction of dissolved oxygen and carbon dioxide concentration profiles in tubular photobioreactors for microalgal culture. *Biotechnol. Bioeng.* **1999**, *62*, 71–86.
- (48) Siemieniuch, J. L.; Gladwell, I. Analysis of explicit difference methods for a diffusion–convection equation. *Int. J. Numer. Methods Eng.* **1978**, *12*, 899–916.
- (49) Sousa, E. The controversial stability analysis. *Appl. Math. Comput.* **2003**, *145*, 777–794.